Energy cost for controlling complex networks with linear dynamics

Gaopeng Duan,[1,2,*] Aming Li,[3,4,*] Tao Meng,[1] Guofeng Zhang,[2] and Long Wang[1,†]
[1]*Center for Systems and Control, College of Engineering, Peking University, Beijing 100871, China*
[2]*Department of Applied Mathematics, Hong Kong Polytechnic University, Hong Kong*
[3]*Department of Zoology, University of Oxford, Oxford OX1 3PS, United Kingdom*
[4]*Chair of Systems Design, Department of Management, Technology and Economics, ETH Zürich, Weinbergstrasse 56/58, Zürich CH-8092, Switzerland*

(Received 20 October 2018; published 21 May 2019)

Examining the controllability of complex networks has received much attention recently. The focus of many studies is commonly trained on whether we can steer a system from an arbitrary initial state to any final state within finite time with admissible external inputs. In order to accomplish the control at the minimum cost, we must study how much control energy is needed to reach the desired state. At a given control distance between the initial and final states, existing results have offered the scaling behavior of lower bounds of the minimum energy in terms of the control time. However, to reach an arbitrary final state at a given control distance, the minimum energy is actually dominated by the upper bound, whose analytic expression still remains elusive. Here we theoretically show the scaling behavior of a precise upper bound of the minimum energy in terms of the time required to achieve control. Apart from validating the analytical results with numerical simulations, our findings are applicable to any number of nodes that receive inputs directly and any types of networks with linear dynamics. Moreover, more precise analytical results for the lower bound of the minimum energy are derived with the proposed method. Our results pave the way for implementing realistic control over various complex networks with the minimum control cost.

DOI: 10.1103/PhysRevE.99.052305

I. INTRODUCTION

An ultimate goal of studying complex systems is to control them on the basis of the underlying topological structures, where nodes indicate units of a system and edges capture who interacts with whom [1–8]. Indeed, by implementing appropriate external control signals, if we can drive a system from an arbitrary initial state to any final state in finite time, we define that the system is controllable, i.e., in principle, we are able to steer a controllable system along our expectations. Recently, the problem of finding a minimal number of nodes that receive external inputs directly to make a network controllable has been investigated [9,10]. Several important results have elucidated important problems pertaining to node classification [11,12], control profiles [13], target control [14], control of edge dynamics [15], as well as the energy (or cost) required for control [16–20] and the corresponding optimal trajectories [21,22].

Beyond the basic property, namely controllability of a system, the control energy steering the system from an initial to a final state has received much attention recently [8,16–20]. Indeed, the energy tells the cost required to pay in practical control, and thus represents another dimension of difficulty in achieving control. Although methods for theoretically approximating the lower bound of control energy and its scaling behavior in terms of the control time have been provided in the literature for both static and temporal networks, the energy to reach an arbitrary final state in phase space is usually dominated by the upper bound [16,20]. In other words, analytical forms on the upper bound of control energy are still missing, and the existing results are all extrapolated from the myriad numerical calculations. In this paper, apart from presenting more precise lower bound of the minimum control energy, we theoretically derive a precise upper bound for the first time. Note that the precise upper bound is the maximum value of all the minimum control energy over all control directions. Furthermore, we show the scaling behavior of both bounds, and offer numerical validations for both cases.

II. THE MINIMUM ENERGY FOR CONTROLLING COMPLEX NETWORKS

Here we consider the linear time-invariant dynamics

$$\dot{\mathbf{x}}(t) = \mathbf{A}\mathbf{x}(t) + \mathbf{B}\mathbf{u}(t), \tag{1}$$

where $\mathbf{x}(t) = [x_1(t)\, x_2(t)\, \ldots\, x_n(t)]^T$ is the state of the whole network with $x_i(t)$ capturing the state of node i; $\mathbf{u}(t) = [u_1(t)\, u_2(t)\, \ldots\, u_m(t)]^T$ is the control input; $\mathbf{A} = (a_{ij})_{nn}$ is the adjacent matrix of the network; $\mathbf{B} = (b_{ij})_{nm}$ is the input matrix with size $n \times m$; and the entry at row i and column j is b_{ij}, being 1 if node i receives the external control input signal $u_j(t)$ directly (driver node), being 0 otherwise.

The networked system (1) is said to be controllable, if it can be driven from any initial state $\mathbf{x}_0 = \mathbf{x}(t_0)$ toward any target state $\mathbf{x}_f = \mathbf{x}(t_f)$ at a given control time t_f, and the corresponding input control energy cost is defined as

*These authors contributed equally to this work.
†Corresponding author: longwang@pku.edu.cn

$E(t_0,t_f)=\int_{t_0}^{t_f}\|\mathbf{u}(t)\|^2dt$ with $\|\mathbf{u}(t)\|$ being the Euclidean norm of the vector $\mathbf{u}(t)$. To minimize the above energy cost, one can adopt the optimal energy control input $\mathbf{u}^*(t)=\mathbf{B}^Te^{\mathbf{A}^T(t_f-t)}\mathbf{G}^{-1}\delta$ with $\mathbf{G}=\int_{t_0}^{t_f}e^{\mathbf{A}(t-t_0)}\mathbf{B}\mathbf{B}^Te^{\mathbf{A}^T(t-t_0)}dt$ and $\delta=\mathbf{x}_f-e^{\mathbf{A}t_f}\mathbf{x}_0$ [23,24], which gives the minimum energy cost $E(t_f)=\delta^T\mathbf{G}^{-1}\delta$ from $\mathbf{x}_0$ to $\mathbf{x}_f$. By assuming $t_0=0$ and $\mathbf{x}_0=\mathbf{0}$ for simplicity, we obtain the minimum energy

$$E(t_f)=\mathbf{x}_f^T\mathbf{G}^{-1}\mathbf{x}_f \tag{2}$$

and note that here the Gramian matrix $\mathbf{G}$ is positive definite when system (1) is controllable [25]. Note that when we refer to control energy later, we mean the minimum control energy. Clearly, for the normalized control distance $\|\mathbf{x}_f\|=1$ we have

$$\frac{1}{\lambda_{\max}(\mathbf{G})}\leqslant E(t_f)\leqslant\frac{1}{\lambda_{\min}(\mathbf{G})}. \tag{3}$$

In what follows, for ease of presenting our framework, we consider undirected networks, and thus $\mathbf{A}$ is a real symmetric matrix accordingly. Subsequently, we have $\mathbf{A}=\mathbf{P}\Xi\mathbf{P}^T$ with $\mathbf{P}\mathbf{P}^T=\mathbf{P}^T\mathbf{P}=\mathbf{I}$, where $\mathbf{P}=(p_{ij})_{nn}$, $\Xi=\mathrm{diag}(\lambda_1,\lambda_2,\ldots,\lambda_n)$, and $\lambda_i,(i=1,2,\ldots,n)$ is the eigenvalue of $\mathbf{A}$ with the ascending order $\lambda_1\leqslant\lambda_2\leqslant\cdots\leqslant\lambda_n$. By letting $\mathbf{Q}=\mathbf{P}^T\mathbf{B}\mathbf{B}^T\mathbf{P}=(q_{ij})_{nn}$ and $\mathbf{F}=(f_{ij})_{nn}$ with $f_{ij}=\frac{1}{\lambda_i+\lambda_j}[e^{(\lambda_i+\lambda_j)t_f}-1]$, we have $\int_0^{t_f}e^{\Xi t}\mathbf{P}^T\mathbf{B}\mathbf{B}^T\mathbf{P}e^{\Xi t}dt=(q_{ij}f_{ij})_{nn}$. Note that the limit of f_{ij} is t_f as $\lambda_i+\lambda_j\to0$, which keeps the above expression of f_{ij} alive when $\lambda_i+\lambda_j=0$. Furthermore, we can calculate $\mathbf{G}$ by

$$\mathbf{G}=\mathbf{P}\int_0^{t_f}e^{\Xi t}\mathbf{P}^T\mathbf{B}\mathbf{B}^T\mathbf{P}e^{\Xi t}dt\mathbf{P}^T=\mathbf{P}\mathbf{M}\mathbf{P}^T, \tag{4}$$

where $\mathbf{M}=(m_{ij})_{nn}$ with $m_{ij}=q_{ij}f_{ij}$. Based on similarity between matrices $\mathbf{G}$ and $\mathbf{M}$, we know that they have the same eigenvalues. Therefore, by calculating the eigenvalues of $\mathbf{M}$ we can find the lower and upper bounds of the minimum energy $E(t_f)$ given in Eq. (3).

III. RESULTS

As discussed in the previous section, driver nodes are nodes who receive external control inputs directly. In this section, for different numbers of driver nodes, we derive the analytical bounds of the control energy separately. For simplicity, here we assume that each single input only injects on a single driver node, and each node only receives an input at most.

A. *n* driver nodes

In the case of n driver nodes, i.e., all nodes receive external inputs directly, we have $m=n$ and $\mathbf{B}=\mathbf{Q}=\mathbf{I}$, which leads to a diagonal matrix $\mathbf{M}$ with $m_{ii}=f_{ii}$. According to the magnitude of the control time t_f, the corresponding bounds are given as follows.

When t_f is small, we have $e^{2\lambda_it_f}\approx1+2\lambda_it_f$, and all eigenvalues of $\mathbf{M}$ can be approximated by t_f. Then both the upper and lower bounds of the minimum energy are t_f^{-1} (see Fig. 1).

When t_f is large and $\mathbf{A}$ is indefinite (ID), i.e., $\lambda_{i-1}<0,\lambda_i=\cdots=\lambda_{i+j}=0,\ 0<\lambda_{i+j+1}$, the pth eigenvalue of $\mathbf{M}$ is given by: (i) $\frac{1}{2|\lambda_p|}$ for $p=1,2,\ldots,i-1$; (ii) t_f for $p=i,i+1,\ldots,i+j$; and (iii) $\frac{e^{2\lambda_pt_f}-1}{2\lambda_p}$ for $p=i+j+1,\ldots,n$. Therefore, we have $\lambda_{\max}(\mathbf{M})=\frac{e^{2\lambda_nt_f}-1}{2\lambda_n}$ and $\lambda_{\min}(\mathbf{M})\approx\frac{1}{2|\lambda_1|}$ with large t_f, which tell that the upper bound $\overline{E}\approx2|\lambda_1|$ and the lower bound $\underline{E}=\frac{2\lambda_n}{e^{2\lambda_nt_f}-1}\sim e^{-2\lambda_nt_f}\to0$.

Similarly, for large t_f, when $\mathbf{A}$ is negative definite (ND, $\lambda_i<0$), $m_{ii}=\frac{e^{2\lambda_it_f}-1}{2\lambda_i}\approx\frac{-1}{2\lambda_i}$ holds. Therefore, all eigenvalues of $\mathbf{M}$ are approximately $\frac{1}{2|\lambda_i|},i=1,2,\ldots,n$, respectively. Then we can obtain the upper bound of energy cost $\overline{E}\approx2|\lambda_1|$ and the lower bound of energy cost $\underline{E}\approx2|\lambda_n|$. When $\mathbf{A}$ is negative semidefinite (NSD, $\lambda_{i-1}<0,\lambda_i=\cdots=\lambda_n=0$), all eigenvalues of $\mathbf{M}$ approximate $\frac{1}{|2\lambda_1|},\frac{1}{|2\lambda_2|},\ldots,\frac{1}{|2\lambda_{i-1}|},\ t_f,t_f,\ldots,t_f$, respectively. Therefore, $\lambda_{\max}(\mathbf{M})=t_f$ and $\lambda_{\min}(\mathbf{M})\approx\frac{1}{2|\lambda_1|}$ with large t_f. Then $\overline{E}\approx2|\lambda_1|$ and $\underline{E}=\frac{1}{t_f}$. When $\mathbf{A}$ is positive semidefinite (PSD, $\lambda_1=\cdots=\lambda_{i-1}=0,0<\lambda_i$), all eigenvalues of $\mathbf{M}$ are $t_f,t_f,\ldots,t_f,\frac{e^{2\lambda_it_f}-1}{2\lambda_i},\frac{e^{2\lambda_{i+1}t_f}-1}{2\lambda_{i+1}},\ldots,\frac{e^{2\lambda_nt_f}-1}{2\lambda_n}$. Thus $\lambda_{\max}(\mathbf{M})=\frac{e^{2\lambda_nt_f}-1}{2\lambda_n}\sim e^{2\lambda_nt_f}$ and $\lambda_{\min}(\mathbf{M})=t_f$ for large t_f. Accordingly, the upper bound of energy is $\overline{E}=t_f^{-1}$ and the lower bound is $\underline{E}=\frac{2\lambda_n}{e^{2\lambda_nt_f}-1}\sim e^{-2\lambda_nt_f}$. When $\mathbf{A}$ is positive definite (PD, $0<\lambda_i$), all eigenvalues of $\mathbf{M}$ are $\frac{e^{2\lambda_1t_f}-1}{2\lambda_1},\frac{e^{2\lambda_2t_f}-1}{2\lambda_2},\ldots,\frac{e^{2\lambda_nt_f}-1}{2\lambda_n}$. Obviously, $\lambda_{\max}(\mathbf{M})=\frac{e^{2\lambda_nt_f}-1}{2\lambda_n}$ and $\lambda_{\min}(\mathbf{M})=\frac{e^{2\lambda_1t_f}-1}{2\lambda_1}$. Consequently, $\overline{E}=\frac{2\lambda_1}{e^{2\lambda_1t_f}-1}\sim e^{-2\lambda_1t_f}$ and $\underline{E}=\frac{2\lambda_n}{e^{2\lambda_nt_f}-1}\sim e^{-2\lambda_nt_f}$.

All of the above analytical scaling laws are confirmed by numerical simulations (Fig. 1).

B. One driver node

In the case of one driver node, the scaling behavior of the lower bound $\underline{E}$ is given in Ref. [16], in which the maximum eigenvalue of $\mathbf{G}$ is approximated by the trace of $\mathbf{G}$. In order to analytically obtain both the upper and lower bounds of the control energy E shown in (3), we adopt the approach presented in Ref. [26] to approximate the maximum and minimum eigenvalues of $\mathbf{M}$ by

$$\lambda_{\max}(\mathbf{M})\approx f(\overline{\alpha},\overline{\beta}) \tag{5}$$

and

$$\lambda_{\min}(\mathbf{M})\approx\frac{1}{f(\underline{\alpha},\underline{\beta})}, \tag{6}$$

where $f(\alpha,\beta)=\sqrt{\frac{\alpha}{n}+\sqrt{\frac{n-1}{n}(\beta-\frac{\alpha^2}{n})}}$, $\overline{\alpha}=\mathrm{trace}(\mathbf{M}^2)$, $\overline{\beta}=\mathrm{trace}(\mathbf{M}^4)$, $\underline{\alpha}=\mathrm{trace}[(\mathbf{M}^{-1})^2]$, and $\underline{\beta}=\mathrm{trace}[(\mathbf{M}^{-1})^4]$. From Fig. 2(a), we can see that it is feasible to employ (5) and (6) to approximate respectively the maximum and the minimum eigenvalues of the real symmetric matrix with high accuracy. Specially, for positive definite matrix $\mathbf{G}$, the accuracy is more pronounced, as shown in Figs. 2(b) and 2(c).

In the literature, it is common to use the trace of $\mathbf{G}$ to estimate the maximum eigenvalue of $\mathbf{G}$ [16,20]. For the lower bound of E, we make a comparison of the precision between the existing result and the result obtained in this paper. From Fig. 3, we find that the lower bounds derived in this paper are more exact.

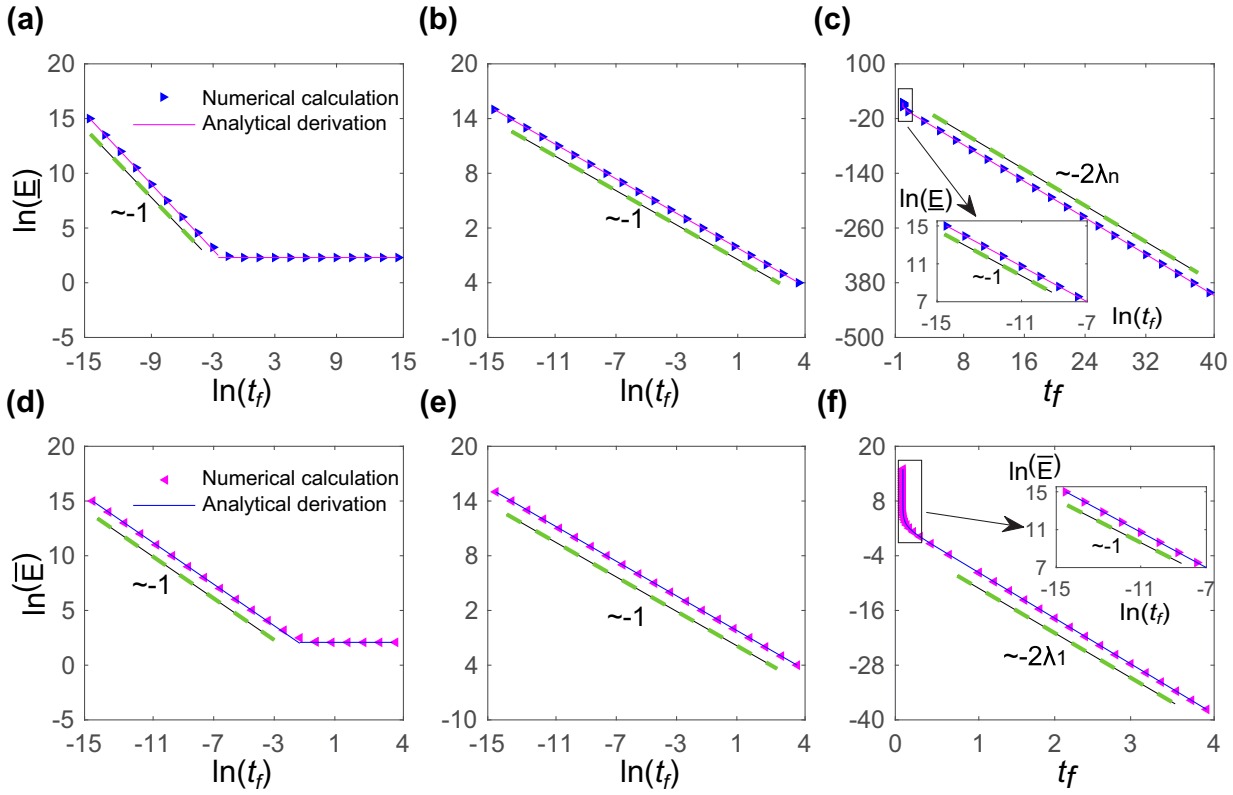

FIG. 1. The lower and upper bounds of control energy for n driver nodes. By controlling all nodes directly, here we show the numerical and analytical results for lower ($\underline{E}$) and upper ($\overline{E}$) bounds of control energy for different types of $\mathbf{A}$. To adjust the maximum (minimum) eigenvalue of $\mathbf{A}$ intuitively, we set the link weight a_{ij} uniformly from $[0, 1]$ in (a) to (d) and from $[-1, 0]$ in (e) and (f); each self-loop (diagonal element) is set as $a + s_i$ with $s_i = -\sum_{j=1}^{n} a_{ij}$. In (a), we set $a = -5$, which guarantees $\mathbf{A}$ is ND with eigenvalues in $[-14.0266, -5]$. Similarly, in (b), $a = 0$ and $\mathbf{A}$ is NSD with eigenvalues in $[-8.5243, 0]$. In (c) and (d), we have $a = 5$, and $\mathbf{A}$ is ID with eigenvalues in $[-4.0266, 5]$. In (e), we set $a = 0$, and hence $\mathbf{A}$ is PSD with all eigenvalues in $[0, 8.3062]$. In (f), $a = 5$ and $\mathbf{A}$ is PD with all eigenvalues in $[5, 13.7144]$. In each panel, triangles (blue and purple) represent results obtained by numerical calculations and full lines indicate analytical derivations under our framework (see Sec. III A and Table I). For small t_f, from each panel with horizontal axis $\ln(t_f)$, we see that all slopes are -1, which confirm our analytical results that both $\overline{E}$ and $\underline{E}$ approximate $\frac{1}{t_f}$ for different types of $\mathbf{A}$. For large t_f, subgraphs with horizontal axis t_f or $\ln(t_f)$ show the analytical scaling behaviors of the bounds of energy precisely. Here we adopt the BA scale-free network with $n = 50$, and network is constructed based on the preferential attachment with average degree 5.8 [27].

By (3) with (5) and (6), we have

$$\overline{E} \approx f(\underline{\alpha}, \underline{\beta}) \tag{7}$$

and

$$\underline{E} \approx \frac{1}{f(\overline{\alpha}, \overline{\beta})}. \tag{8}$$

With only one driver node, we denote the node h as the sole driver node with $b_{h1} = 1$ and $b_{i1} = 0 (i \neq h)$. Since $m_{ij} = q_{ij} f_{ij}$ and $q_{ij} = p_{hi} p_{hj}$, we obtain $m_{ij} = \frac{p_{hi} p_{hj}}{\lambda_i + \lambda_j} [e^{(\lambda_i + \lambda_j) t_f} - 1]$. Furthermore, we have $\mathbf{M}^2(i, i) = \sum_{k=1}^{n} \frac{p_{hk}^2 p_{hi}^2}{(\lambda_k + \lambda_i)^2} [e^{(\lambda_k + \lambda_i) t_f} - 1]^2$ and $\mathbf{M}^4(i, i) = \sum_{l=1}^{n} \{\sum_{k=1}^{n} \frac{p_{hk}^2 p_{hi} p_{hl}}{(\lambda_k + \lambda_i)(\lambda_k + \lambda_l)} [e^{(\lambda_k + \lambda_i) t_f} - 1][e^{(\lambda_k + \lambda_l) t_f} - 1]\}^2$. Note that $\mathrm{trace}(£^2) = \|£\|_F$ for arbitrary square matrix £. Then, we get the values of $\overline{\alpha}$ and $\overline{\beta}$ as

$$\overline{\alpha} = \mathrm{trace}(\mathbf{M}^2) = \sum_{i=1}^{n} \sum_{k=1}^{n} \frac{p_{hk}^2 p_{hi}^2}{(\lambda_k + \lambda_i)^2} [e^{(\lambda_k + \lambda_i) t_f} - 1]^2 \tag{9}$$

and

$$\begin{aligned} \overline{\beta} &= \mathrm{trace}(\mathbf{M}^4) \\ &= \sum_{i=1}^{n} \sum_{l=1}^{n} \left\{ \sum_{k=1}^{n} \frac{p_{hk}^2 p_{hi} p_{hl}}{(\lambda_k + \lambda_i)(\lambda_k + \lambda_l)} \right. \\ &\quad \left. \cdot [e^{(\lambda_k + \lambda_i) t_f} - 1][e^{(\lambda_k + \lambda_l) t_f} - 1] \right\}^2. \end{aligned} \tag{10}$$

Based on Eqs. (9) and (10), we have discussed and calculated the parameters $\overline{\alpha}$ and $\overline{\beta}$ in different cases (see Table III). Besides, $\underline{\alpha}$ and $\underline{\beta}$ have also been obtained in different cases (see Table IV). Accordingly, the upper and lower bounds of energy cost are given in Tables I and II, and numerical validations of our analytical results are shown in Fig. 4.

C. *d* driver nodes

In the case of d driver nodes, we label them $m_1, m_2, \ldots, m_d$. Hence $\mathbf{B} = [e_{m_1}, e_{m_2}, \ldots, e_{m_d}] \in R^{n \times d}$, where $e_i = (0 \ldots 0\ 1\ 0 \ldots 0)^T \in R^n$ with all elements as

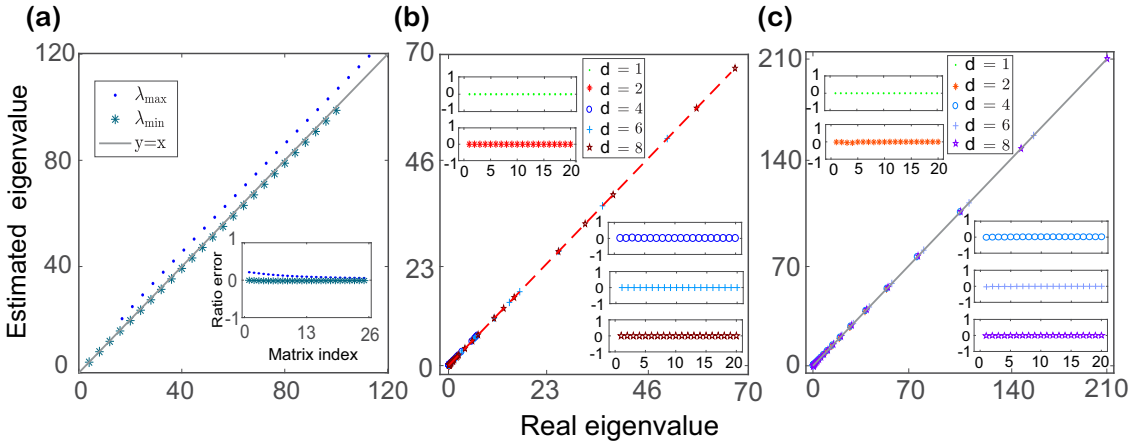

FIG. 2. Veracity of eigenvalues estimation based on Eqs. (5) and (6). In (a), we randomly generate 25 matrices with minimum eigenvalue being $4i$, $i = 1, 2, \ldots, 25$, where i is the index of the matrix. The horizontal and vertical coordinates represent the true eigenvalues and estimated eigenvalues by Eqs. (5) and (6), from which it is clear the generated pattern almost overlaps with $y = x$. The inset presents ratio errors of differences between approximated eigenvalues by Eqs. (5) and (6) and the true eigenvalues, which indicates the accuracy of estimation is reliable, especially the estimation of minimum eigenvalues by (6). In (b) and (c), we make estimations of the maximum and the minimum eigenvalues of the matrix $\mathbf{G}$ for the case of d driver nodes. All validations are carried out on BA networks with 10 nodes. To be more persuasive, we set the number of driver nodes denoted by d as 1, 2, 4, 6, 8, respectively. And for BA networks, all cases of the different $\mathbf{A}$ with different properties (ND, NSD, ID, PD, PSD) are considered. In (b), the horizontal axis represents the real minimum eigenvalue of $\mathbf{M}$, and the vertical axis represents the estimated value by (6), where we set $\mathbf{A}$ as PD, PSD, not PD by selecting a_{ij} from $[-4, -1]$ uniformly and a from -4 to 4 with an interval 0.2. In (c), the horizontal axis represents the real maximum eigenvalue of $\mathbf{M}$, and the vertical axis represents the estimated value by (5), where we set $\mathbf{A}$ as ND, NSD, not ND by uniformly selecting a_{ij} from $[1, 3]$ and a from -4 to 4 with an interval 0.2. Subplots present the ratio error similar to those in (a) with half original data, where the horizontal axis presents the matrix index and the vertical axis indicates the ratio error.

0, except the ith element as 1. Let $\mathbf{P}_1 = \mathbf{B}^T\mathbf{P}$, where $\mathbf{P}_1$ is a $d \times n$ matrix constituted by the rows $m_1, m_2, \ldots, m_d$ of $\mathbf{P}$. Thus $\mathbf{Q} = \mathbf{P}_1^T\mathbf{P}_1$ with $q_{ij} = \sum_{k=1}^{d} p_{m_k i} p_{m_k j}$. By comparing the form of $m_{ij} = q_{ij} f_{ij}$ between the cases of one driver node and d driver nodes, we find that only the form of q_{ij} is different. Therefore, in subsequent analysis and calculation, we can refer to Sec. III B to derive $\overline{\alpha}$ and $\overline{\beta}$ (see Appendix B for details). We summarize the lower bound of energy under d driver nodes for different scenarios in Table I and the corresponding numerical validations are presented in Fig. 5. In addition, the upper bound of energy is presented in Table II.

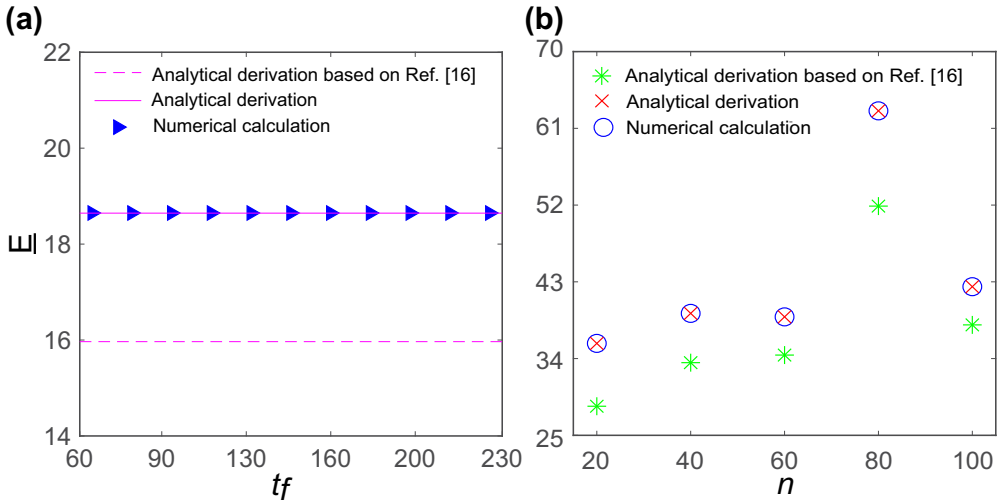

FIG. 3. The lower bound of energy comparisons between the methods shown in Ref. [16] and this paper. Here we randomly generate BA scale-free networks with $\mathbf{A}$ being ND (other parameters are the same as those in Fig. 1) and a_{ij} is selected from $[1, 3]$ uniformly with $a = -2$. For approximating the maximum eigenvalue of $\mathbf{M}$, here we use the method shown in (5), while in Ref. [16], it is inferred by the corresponding trace. Since the existing results only consider the scenario for one driver node, we follow this setting. In (a), the network size is set as 10. In (b), the analytically derived and numerical lower bounds of E are depicted at $t_f = 200$ for different network sizes (n) accordingly. For all cases, we can see that the method we employed generates much more precise $\underline{E}$ compared to the existed tools.

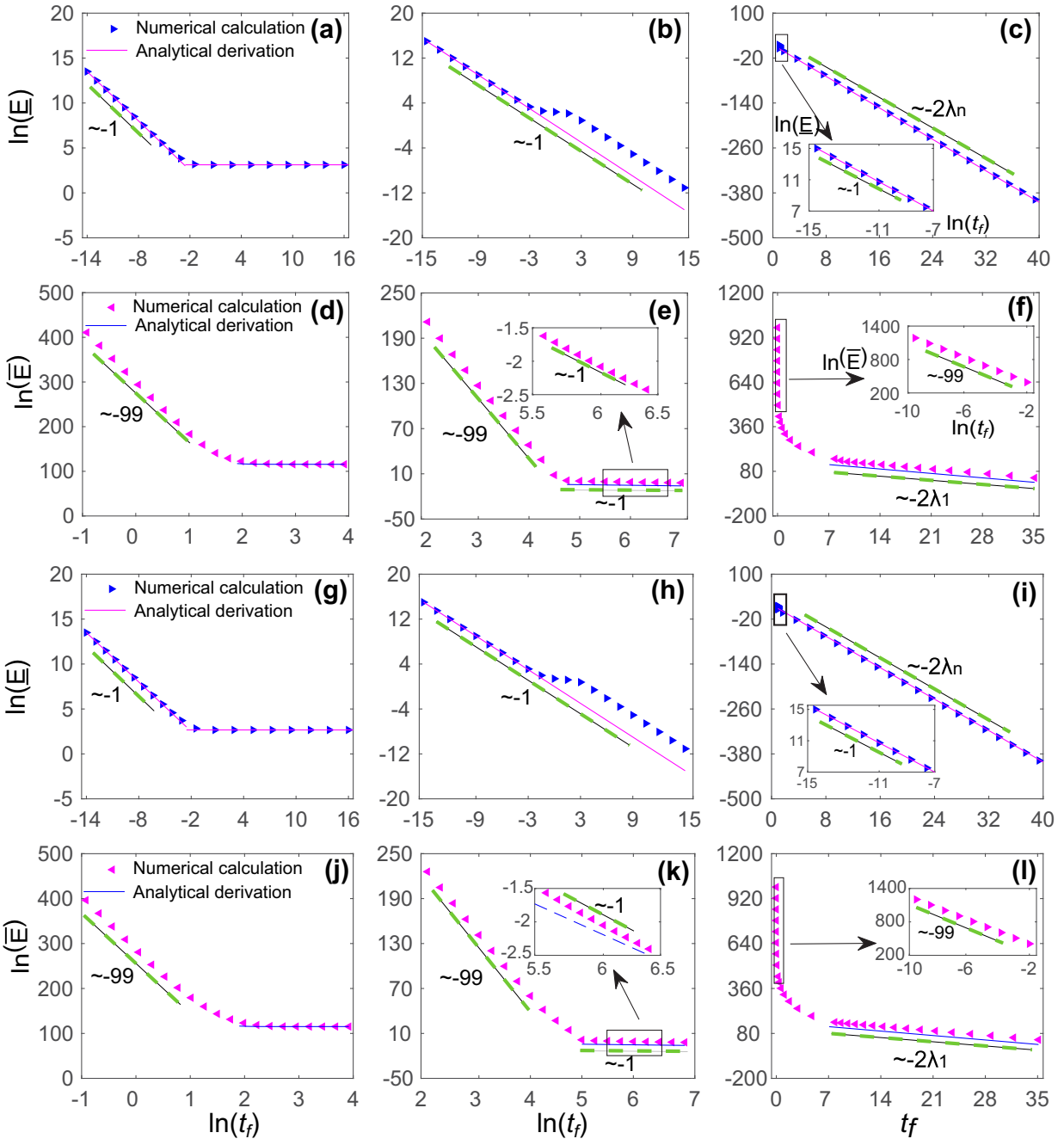

FIG. 4. The lower and upper bounds of energy for one driver node. The scaling behavior of the lower and upper bounds of energy cost is given for one driver node, and the summation of analytical results are presented in Tables I and II. For scale-free networks in (a)–(f) and random networks in (g)–(l), all parameters are the same except that the network structure is different. In (a)–(c), with small t_f, $\underline{E} \sim t_f^{-1}$ for all $\mathbf{A}$. In (d)–(f) for upper bound, the slope of triangular trajectory is much less than -1. Parameters are selected the same as those given in Fig. 1. The interval of the uniform distribution is $[0, 1]$ in (a)–(c), $[1, 3]$ in (d), $[-1, 0]$ in (e), and $[-5, -2]$ in (f). In (a), $a = -5$, by which $\mathbf{A}$ is ND with eigenvalues in $[-14.0266, -5]$. Similarly, in (b) and (e), $a = 0$ such that $\mathbf{A}$ is NSD and PSD, respectively. In (c) and (d), $a = 5$ such that $\mathbf{A}$ is ID. In (f), $a = 3$, such that the minimum eigenvalue of $\mathbf{A}$ is 3. In (g)–(l), the probability for adding an edge between every randomly selected pair nodes is 0.1 [29].

IV. DISCUSSION

In this paper, we have investigated the scaling behavior of the bounds of minimum control energy for controlling complex networks in terms of the time given to achieve control. The bounds of minimum energy are determined by the maximum and the minimum eigenvalues of $\mathbf{G}$. The maximum eigenvalue is usually approximated by the trace of $\mathbf{G}$, while the approximation of the corresponding minimum eigenvalue has not been discussed until now. Here we employ an effective method which not only provides more precise analytical expression than the conventional trace for approximating the

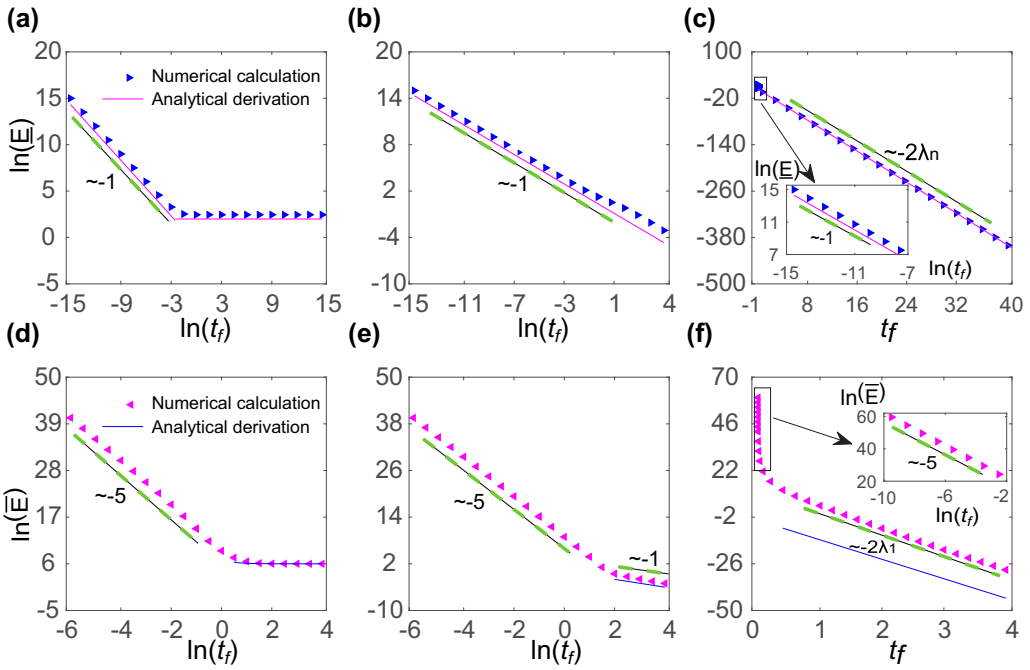

FIG. 5. The lower and upper bounds of control energy for 20 driver nodes. In (a)–(c), with small t_f, $\underline{E} \sim t_f^{-1}$ for all **A**. In (d)–(f) for upper bound, the slope of triangular trajectory is much less than -1. The summation of the analytical results are presented in Tables I and II. Parameters are selected as those given in Fig. 1. The interval of uniform distribution is $[0, 1]$ in (a)–(d), and $[-1, 0]$ in (e) and (f). In (a), $a = -5$, by which **A** is ND with eigenvalues in $[-12.5048, -5]$. Similarly, in (b) and (e), $a = 0$ such that **A** is NSD and PSD, respectively. In (c) and (d), $a = 5$ such that **A** is ID. Similarly, $a = 5$ such that **A** is PD.

maximum eigenvalue, but also shows the analytical form of the minimum eigenvalues. Besides, all the derived theoretical laws are confirmed by numerical simulations.

Our framework also applies to weighted directed networks. When system (1) is controllable, the matrix **G** is positive definite. When **A** is asymmetrical for directed networks, we can still obtain the specific form of **G**. Based on **G**, the lower bound of energy cost can be calculated by Eq. (8) with the traces of $\mathbf{G}^2$ and $\mathbf{G}^4$. For the upper bound of energy cost, we can apply the method proposed in this paper to get the scaling behavior of energy by the inverse of **G** (see Appendix A).

Although natural systems are believed to operate with nonlinear dynamics, the type of nonlinearity and empirical parameterization are usually hard to detect, especially for large systems. Besides, the generality cannot be guaranteed for results obtained from some specific nonlinear systems. In contrast, the linear dynamics we analyzed here allows us to derive the theoretical insights, which are normally suitable for analyzing various complex networks. In general, the

TABLE I. The lower bound of control energy $\underline{E}$. No matter how many driver nodes there are, for small t_f, $\underline{E} \sim t_f^{-1}$. For large t_f, when **A** is ND (negative definite), $\underline{E}$ approaches a constant irrespective of t_f, (C_1 for one driver node, C_2 for d driver nodes and $2|\lambda_n|$ for n driver nodes), where C_1 and C_2 are given as Eq. (8) with Eqs. (A1) and (A2) and with Eqs. (B3) and (B4), respectively. When **A** is NSD (negative semidefinite) with large t_f, $\underline{E} \approx t_f^{-1}$ under n driver nodes; while it approaches t_f^{-1} for one and d driver nodes [detailed forms are given as Eq. (8) with Eqs. (A5) and (A6) and with Eqs. (B5) and (B6), respectively]. In addition, when **A** is not ND (including the cases of indefinite, positive semidefinite, and positive definite), $\underline{E} \sim e^{-2\lambda_n t_f}$ holds for large t_f.

Number of driver nodes		1	d	n
Small t_f		$\sim t_f^{-1}$	$\sim t_f^{-1}$	t_f^{-1}
Large t_f	ND	C_1	C_2	$2\lvert\lambda_n\rvert$
	NSD	$\sim t_f^{-1}$	$\sim t_f^{-1}$	t_f^{-1}
	Not ND	$\sim e^{-2\lambda_n t_f}$	$\sim e^{-2\lambda_n t_f}$	$\sim e^{-2\lambda_n t_f}$

TABLE II. The upper bound of control energy $\overline{E}$. For small t_f, both $N_0 - N_{\min}$ and $N_0' - N_{\min}'$ are much larger than 1, where the detailed meanings of N_0, $N_{\min}$, N_0', and $N_{\min}'$ are given in Appendices A and B. For large t_f, when **A** is PD (positive definite), $\overline{E} \sim e^{-2\lambda_1 t_f}$ for arbitrary number of driver nodes; when **A** is PSD (positive semidefinite), $\overline{E} \sim t_f^{-1}$; when **A** is not PD (including the cases of indefinite, negative semidefinite, and negative definite), $\overline{E}$ approaches to a constant irrespective of the magnitude of t_f for large t_f (C_3 for one driver node, C_4 for d driver nodes, and $2|\lambda_1|$ for n driver nodes), where C_3 has different forms for different **A** (detailed forms are presented in Table IV).

Number of driver nodes		1	d	n
Small t_f		$\sim t_f^{-(N_0 - N_{\min})}$	$\sim t_f^{-(N_0' - N_{\min}')}$	t_f^{-1}
Large t_f	PD	$\sim e^{-2\lambda_1 t_f}$	$\sim e^{-2\lambda_1 t_f}$	$\sim e^{-2\lambda_1 t_f}$
	PSD	$\sim t_f^{-1}$	$\sim t_f^{-1}$	t_f^{-1}
	Not PD	C_3	C_4	$2\lvert\lambda_1\rvert$

linear dynamics is important to explore nonlinear systems by investigating the linearized version of nonlinear dynamics. Indeed, if the linearized dynamics of a nonlinear system is controllable along some trajectory, then the nonlinear system is locally controllable along the same trajectory [28]. Nevertheless, it is worth investigating nonlinear dynamics or possible revisions with nonlinearity over linear dynamics in subsequent research. Even that we only consider static complex networks, our framework can also be extended to explore the bounds of energy cost for controlling temporal networks by virtue of the effective Gramian matrix given in Ref. [8]. Specifically, by utilizing the estimations of both maximum and minimum eigenvalues and some approximate techniques introduced in this paper, the scaling behavior of the energy cost for controlling temporal networks [8] can be obtained conveniently.

ACKNOWLEDGMENTS

This work is supported by the National Natural Science Foundation of China (NSFC) under Grants No. 61751301 and No. 61533001. A.L. acknowledges the support from the Human Frontier Science Program Postdoctoral Fellowship (Grant No. LT000696/2018-C), the Foster Lab at Oxford, and the Chair of Systems Design at ETH Zürich. G.Z. acknowledges the financial support from the Hong Kong Research Grant council (RGC) (Grants No. 15206915 and No. 15208418).

APPENDIX A: ONE DRIVER NODE

In the case of one driver node, we can obtain lower bound of energy cost (8) by calculating $\overline{\alpha}$ and $\overline{\beta}$. For the upper bound of energy cost (7), we apply (6) to estimate the minimum eigenvalue of $\mathbf{M}$. In the analysis process, the key step is to get $\mathbf{M}^{-1}$. In what follows, we make detailed explanation according to the magnitude of t_f.

1. Small t_f

For small t_f, the expected numbers of $\overline{\alpha}$ and $\overline{\beta}$ are $\overline{\alpha} \approx \sum_{i=1}^{n}\sum_{k=1}^{n} p_{hk}^2 p_{hi}^2 t_f^2$ and $\overline{\beta} \approx \sum_{i=1}^{n}\sum_{l=1}^{n}\left(\sum_{k=1}^{n} p_{hk}^2 p_{hi} p_{hl}\right)^2 t_f^4$, where we use $e^{(\lambda_i+\lambda_j)t_f} \approx 1+(\lambda_i+\lambda_j)t_f$ for small t_f. Hence, we have $\underline{E} \sim t_f^{-1}$.

Accordingly, we get

$$\mathbf{M} \approx t_f \cdot \begin{bmatrix} p_{h1}^2 & p_{h1}p_{h2} & \cdots & p_{h1}p_{hn} \\ p_{h1}p_{h2} & p_{h2}^2 & \cdots & p_{h2}p_{hn} \\ \vdots & \vdots & \ddots & \vdots \\ p_{h1}p_{hn} & p_{h2}p_{hn} & \cdots & p_{hn}^2 \end{bmatrix}$$

and by imposing the row elementary transformation on $\mathbf{M}$, we have

$$\mathbf{M} \to t_f \cdot \begin{bmatrix} p_{h1}^2 & p_{h1}p_{h2} & \cdots & p_{h1}p_{hn} \\ 0 & 0 & \cdots & 0 \\ \vdots & \vdots & \ddots & \vdots \\ 0 & 0 & \cdots & 0 \end{bmatrix},$$

meaning that $\mathbf{M}$ is not invertible with the first-order Taylor series expansion.

When $e^{(\lambda_i+\lambda_j)t_f} \approx 1+(\lambda_i+\lambda_j)t_f + \frac{(\lambda_i+\lambda_j)^2}{2}t_f^2$, the corresponding matrix $\mathbf{M}$ is obtained with $m_{ij} = p_{hi}p_{hj}(1+\frac{\lambda_i+\lambda_j}{2}t_f)t_f$. Then we take two row elementary transformations on $\mathbf{M}$ as

$$\Theta_2\Theta_1\mathbf{M} = t_f \cdot \begin{bmatrix} p_{h1}^2(1+\frac{2\lambda_1}{2}t_f) & p_{h1}p_{h2}(1+\frac{\lambda_1+\lambda_2}{2}t_f) & \cdots & p_{h1}p_{hn}(1+\frac{\lambda_1+\lambda_n}{2}t_f) \\ 0 & p_{h2}^2\frac{-(\lambda_1-\lambda_2)^2t_f^2}{4(1+\lambda_1 t_f)} & \cdots & p_{h2}p_{hn}\frac{(\lambda_n-\lambda_1)(\lambda_1-\lambda_2)t_f^2}{4(1+\lambda_1 t_f)} \\ 0 & 0 & \cdots & 0 \\ \vdots & \vdots & \ddots & \vdots \\ 0 & 0 & \cdots & 0 \end{bmatrix}.$$

where Θ_1 and Θ_2 have the following forms:

$$\Theta_1 = \begin{bmatrix} 1 & 0 & 0 & \cdots & 0 \\ * & 1 & 0 & \cdots & 0 \\ * & 0 & 1 & \cdots & 0 \\ \vdots & \vdots & \vdots & \ddots & \vdots \\ * & 0 & 0 & \cdots & 1 \end{bmatrix}, \quad \Theta_2 = \begin{bmatrix} 1 & 0 & 0 & \cdots & 0 \\ 0 & 1 & 0 & \cdots & 0 \\ 0 & * & 1 & \cdots & 0 \\ \vdots & \vdots & \vdots & \ddots & \vdots \\ 0 & * & 0 & \cdots & 1 \end{bmatrix}.$$

In this case, $\mathbf{M}$ also is not invertible with the second-order Taylor series expansion. Hence, we must approximate $e^{(\lambda_i+\lambda_j)t_f}$ via Taylor series $1+(\lambda_i+\lambda_j)t_f + \frac{(\lambda_i+\lambda_j)^2}{2}t_f^2 + \cdots + \frac{(\lambda_i+\lambda_j)^N}{N!}t_f^N$ with large N such that the approximated $\mathbf{M}$ has full rank when $t_f \ll \frac{N!}{(\lambda_i+\lambda_j)^N}$, which is the basis of our subsequent calculations and analysis. Let $\mathbf{M}_{ij}$ denote the algebraic complement of m_{ij}. Afterward, one gets $|\mathbf{M}| \sim t_f^{N_0}$ with $N_0 \gg 1$ and $\mathbf{M}_{ij} \sim t_f^{N_{ij}}$ with $N_{ij} \ll N_0$. Accordingly, $\underline{\alpha}$ and $\underline{\beta}$ satisfy $\underline{\alpha} \sim t_f^{2(N_{\min}-N_0)}$, $\underline{\beta} \sim t_f^{4(N_{\min}-N_0)}$ with $N_{\min} = \min\{N_{ij}|i,j=1,2,\ldots,n\}$. Therefore, we have $\overline{E} \sim t_f^{-(N_0-N_{\min})}$.

2. Large t_f

a. A *is ND*

For large t_f, when **A** is ND, $e^{(\lambda_i+\lambda_j)t_f} \to 0$ holds. Then (9) and (10) are further obtained with

$$\overline{\alpha} \approx \sum_{i=1}^{n}\sum_{j=1}^{n} \frac{p_{hj}^2 p_{hi}^2}{(\lambda_j+\lambda_i)^2}, \tag{A1}$$

$$\overline{\beta} \approx \sum_{i=1}^{n}\sum_{l=1}^{n}\left[\sum_{k=1}^{n} \frac{p_{hk}^2 p_{hi} p_{hl}}{(\lambda_k+\lambda_i)(\lambda_k+\lambda_l)}\right]^2. \tag{A2}$$

And the specific form m_{ij} of **M** is $\frac{-p_{hi}p_{hj}}{\lambda_i+\lambda_j}$ for $\forall\, i, j = 1, 2, \ldots, n$. In addition, we can calculate inverse matrix of **M** as

$$\mathbf{M}^{-1}(i,j) = \frac{-4\lambda_i\lambda_j}{p_{hi}p_{hj}(\lambda_i+\lambda_j)} \prod_{k=1,k\neq i}^{n} \frac{\lambda_i+\lambda_k}{\lambda_i-\lambda_k} \prod_{k=1,k\neq j}^{n} \frac{\lambda_j+\lambda_k}{\lambda_j-\lambda_k}.$$

Further, we have $(\mathbf{M}^{-1})^2$ with

$$(\mathbf{M}^{-1})^2(i,j) = \sum_{r=1}^{n} \frac{16\lambda_r^2\lambda_i\lambda_j}{p_{hr}^2 p_{hi}p_{hj}(\lambda_r+\lambda_i)(\lambda_r+\lambda_j)} \prod_{k=1,k\neq r}^{n} \left(\frac{\lambda_r+\lambda_k}{\lambda_r-\lambda_k}\right)^2 \prod_{k=1,k\neq i}^{n} \frac{\lambda_i+\lambda_k}{\lambda_i-\lambda_k} \prod_{k=1,k\neq j}^{n} \frac{\lambda_j+\lambda_k}{\lambda_j-\lambda_k}.$$

Sequentially, we have

$$\underline{\alpha} = \mathrm{trace}[(\mathbf{M}^{-1})^2] = \sum_{i=1}^{n}\sum_{j=1}^{n} \frac{16\lambda_j^2\lambda_i^2}{p_{hj}^2 p_{hi}^2(\lambda_j+\lambda_i)^2} \prod_{k=1,k\neq j}^{n} \left(\frac{\lambda_j+\lambda_k}{\lambda_j-\lambda_k}\right)^2 \prod_{k=1,k\neq i}^{n} \left(\frac{\lambda_i+\lambda_k}{\lambda_i-\lambda_k}\right)^2 \tag{A3}$$

and

$$\underline{\beta} = \sum_{i=1}^{n}\sum_{j=1}^{n}\left[\sum_{r=1}^{n} \frac{16\lambda_r^2\lambda_i\lambda_j}{p_{hr}^2 p_{hi}p_{hj}(\lambda_r+\lambda_i)(\lambda_r+\lambda_j)} \prod_{k=1,k\neq r}^{n} \left(\frac{\lambda_r+\lambda_k}{\lambda_r-\lambda_k}\right)^2 \prod_{k=1,k\neq i}^{n} \frac{\lambda_i+\lambda_k}{\lambda_i-\lambda_k} \prod_{k=1,k\neq j}^{n} \frac{\lambda_j+\lambda_k}{\lambda_j-\lambda_k}\right]^2. \tag{A4}$$

b. A *is NSD*

For large t_f, when **A** is NSD, with $\lim_{\lambda_i+\lambda_j\to 0} \frac{e^{(\lambda_i+\lambda_j)t_f}-1}{\lambda_i+\lambda_j} = t_f$ and $e^{(\lambda_i+\lambda_j)t_f} \to 0$, we have

$$\overline{\alpha} \approx \sum_{i=1}^{n}\sum_{k=1}^{n} p_{hk}^2 p_{hi}^2 t_f^2 \sim t_f^2 \tag{A5}$$

and

$$\overline{\beta} \approx \sum_{i=1}^{n}\sum_{l=1}^{n}\left(\sum_{k=1}^{n} p_{hk}^2 p_{hi} p_{hl}\right)^2 t_f^4 \sim t_f^4. \tag{A6}$$

And then we can obtain $\underline{E} \sim t_f^{-1}$. Assume $\lambda_1 \leqslant \cdots \leqslant \lambda_l < 0, \lambda_{l+1} = \cdots = \lambda_n = 0$. The elements m_{ij} of the corresponding matrix **M** are $\frac{-p_{hi}p_{hj}}{\lambda_i+\lambda_j}$ for $i \leqslant l,\ j \leqslant l$; $\frac{-p_{hi}p_{hj}}{\lambda_j}$ for $i > l,\ j \leqslant l$; $\frac{-p_{hi}p_{hj}}{\lambda_i}$ for $i \leqslant l,\ j > l$; and $p_{hi}p_{hj}t_f$ for $i > l,\ j > l$. It is easy to get that $|\mathbf{M}| \sim t_f^{n-l}$. With $\mathbf{M}_{ij}$ denoting the algebraic complement of m_{ij}, we can get $\mathbf{M}_{ij} \sim t_f^{n-l}$ for $i \leqslant l, j \leqslant l$ and $\mathbf{M}_{ij} \sim t_f^{n-l-1}$ otherwise. Due to $\mathbf{M}^{-1} = \frac{\mathbf{M}^*}{|\mathbf{M}|}$ with $\mathbf{M}^* = (\mathbf{M}_{ij}) \in R^{n\times n}$, we can derive all elements of $\mathbf{M}^{-1}$ as $\mathbf{M}^{-1}(i,j) \approx c_{ij} \neq 0$, for $i \leqslant l, j \leqslant l$, and $\mathbf{M}^{-1}(i,j) \approx 0$ otherwise, where c_{ij} are constants independent of t_f for all $i, j \leqslant l$. Consequently, $\underline{\alpha} = \mathrm{trace}[(\mathbf{M}^{-1})^2] = \sum_{i=1}^{l}\sum_{j=1}^{l} c_{ij}^2$ is a constant as well as $\underline{\beta}$. In addition, from the above analysis, we find that in calculating $\underline{\alpha}$ and $\underline{\beta}$, only elements $\mathbf{M}^{-1}(i,j), i, j \leqslant l$ are determinant. Therefore, in order to get the specific forms of $\underline{\alpha}$ and $\underline{\beta}$, we apply trace $[(\mathbf{M}_1^{-1})^2]$ and trace $[(\mathbf{M}_1^{-1})^4]$ to appropriate $\underline{\alpha}$ and $\underline{\beta}$, respectively, where $\mathbf{M}_1 = (m_{ij}) \in R^{l\times l}$ with m_{ij} $(i, j \leqslant l)$ being the corresponding element of **M**. Hence, similar to the case of **A** being ND, we can get

$$\begin{aligned}\underline{\alpha} &= \mathrm{trace}[(\mathbf{M}^{-1})^2] \\ &\approx \sum_{i=1}^{l}\sum_{j=1}^{l} \frac{16\lambda_j^2\lambda_i^2}{p_{hj}^2 p_{hi}^2(\lambda_j+\lambda_i)^2} \prod_{k=1,k\neq j}^{n} \left(\frac{\lambda_j+\lambda_k}{\lambda_j-\lambda_k}\right)^2 \\ &\quad \cdot \prod_{k=1,k\neq i}^{n} \left(\frac{\lambda_i+\lambda_k}{\lambda_i-\lambda_k}\right)^2\end{aligned} \tag{A7}$$

and

$$\begin{aligned}\underline{\beta} \approx \sum_{i=1}^{l}\sum_{j=1}^{l}\Bigg[&\sum_{r=1}^{l} \frac{16\lambda_r^2\lambda_i\lambda_j}{p_{hr}^2 p_{hi}p_{hj}(\lambda_r+\lambda_i)(\lambda_r+\lambda_j)} \\ &\cdot \prod_{k=1,k\neq r}^{n} \left(\frac{\lambda_r+\lambda_k}{\lambda_r-\lambda_k}\right)^2 \prod_{k=1,k\neq i}^{n} \frac{\lambda_i+\lambda_k}{\lambda_i-\lambda_k} \\ &\cdot \prod_{k=1,k\neq j}^{n} \frac{\lambda_j+\lambda_k}{\lambda_j-\lambda_k}\Bigg]^2.\end{aligned} \tag{A8}$$

Since $\underline{\alpha}$ and $\underline{\beta}$ presented as (A7) and (A8) are constants independent of t_f, the upper bound of energy cost with NSD **A** is also a constant as shown in (7) with (A7) and (A8).

c. **A** *is ID*

For large t_f, when **A** is ID, by assuming $\lambda_1 \leqslant \cdots \leqslant \lambda_l < 0, \lambda_{l+1} = \cdots = \lambda_{l+r} = 0, 0 < \lambda_{l+r+1} \leqslant \cdots \leqslant \lambda_n$, we have that the component $e^{4\lambda_n t_f}$ of $\overline{\alpha}$ dominates. Thus we get $\overline{\alpha} \approx \frac{p_{hn}^4}{4\lambda_n^2} e^{4\lambda_n t_f}$ and analogously $\overline{\beta} \approx \frac{p_{hn}^8}{16\lambda_n^4} e^{8\lambda_n t_f}$. Then the lower bound of energy cost $\underline{E} \approx \frac{2\lambda_n}{p_{hn}^2} e^{-2\lambda_n t_f}$. And **M** has the form

$$\mathbf{M} = \begin{bmatrix} \mathbf{M}_1 & \mathbf{M}_2 & \mathbf{M}_3 \\ \mathbf{M}_2^T & \mathbf{M}_4 & \mathbf{M}_5 \\ \mathbf{M}_3^T & \mathbf{M}_5^T & \mathbf{M}_6 \end{bmatrix}$$

with

$$\begin{cases} \mathbf{M}_1(i,j) = \frac{-p_{hi}p_{hj}}{\lambda_i+\lambda_j}, & i,j = 1,2,\ldots,l; \\ \mathbf{M}_2(i,j) = \frac{-p_{hi}p_{hj}}{\lambda_i}, & i = 1,2,\ldots,l; \\ & j = l+1,\ldots,l+r; \\ \mathbf{M}_3(i,j) = p_{hi}p_{hj}e^{(\lambda_i+\lambda_j)t_f}, & i = 1,2,\ldots,l; \\ & j = l+r+1,\ldots,n; \\ \mathbf{M}_4(i,j) = p_{hi}p_{hj}t_f, & i,j = l+1,\ldots,l+r; \\ \mathbf{M}_5(i,j) = \frac{-p_{hi}p_{hj}}{\lambda_j}e^{\lambda_j t_f}, & i = l+1,\ldots,l+r; \\ & j = l+r+1,\ldots,n; \\ \mathbf{M}_6(i,j) = \frac{-p_{hi}p_{hj}}{\lambda_i+\lambda_j}e^{(\lambda_i+\lambda_j)t_f}, & i,j = l+r+1,\ldots,n. \end{cases}$$

Note that in current form of $\mathbf{M}_3$, we assume $\lambda_i + \lambda_j > 0$. For other cases, subsequent analysis is not affected, which are omitted here. For large t_f, it is clear that $|\mathbf{M}| \sim e^{2(\lambda_{l+r+1}+\lambda_{l+r+2}+\cdots+\lambda_n)t_f} \cdot t_f^r$. And the algebraic complement of m_{ij} is

$$\mathbf{M}_{ij} \sim \begin{cases} e^{at_f}t_f^r, \text{ with } a = 2(\lambda_{l+r+1}+\cdots+\lambda_n), & i,j < l; \\ e^{bt_f}t_f^c, \text{ with } b < a \text{ or } c < r, & \text{otherwise.} \end{cases}$$

Further, for each element of $\mathbf{M}^{-1}$, we have

$$\mathbf{M}^{-1}(i,j) \approx \begin{cases} c_{ij} \neq 0, & i,j < l; \\ 0, & \text{otherwise.} \end{cases}$$

Similar to the case of **A** being NSD with large t_f, both $\underline{\alpha}$ and $\underline{\beta}$ approximated by the trace$[(\mathbf{M}_1^{-1})^2]$ and trace$[(\mathbf{M}_1^{-1})^4]$, are constants as

$$\begin{aligned} \underline{\alpha} &= \text{trace}[(\mathbf{M}^{-1})^2] \\ &\approx \sum_{i=1}^{l}\sum_{j=1}^{l} \frac{16\lambda_j^2\lambda_i^2}{p_{hj}^2 p_{hi}^2(\lambda_j+\lambda_i)^2} \prod_{k=1,k\neq j}^{n} \left(\frac{\lambda_j+\lambda_k}{\lambda_j-\lambda_k}\right)^2 \\ &\quad \cdot \prod_{k=1,k\neq i}^{n} \left(\frac{\lambda_i+\lambda_k}{\lambda_i-\lambda_k}\right)^2 \end{aligned} \tag{A9}$$

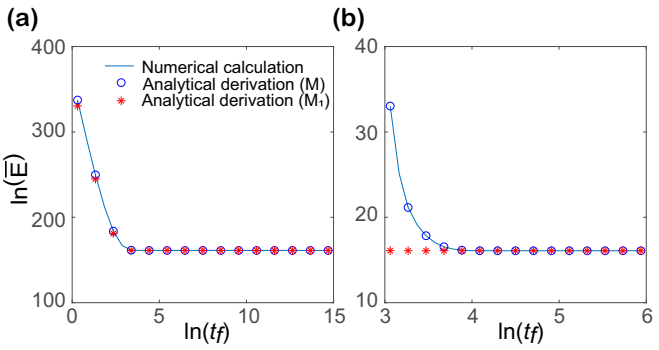

FIG. 6. The upper bound of energy estimated by (7) with $\mathbf{M}_1$ representing **M**. All networks are BA networks with 50 nodes and one driver node. In (a) and (b), with large t_f, $\overline{E}$ converges to the constant when **A** is NSD or ID. And the trajectories of $\overline{E}$ with **M** and $\mathbf{M}_1$ handled are almost coincide. Parameters are selected as those given in Fig. 1. In (a), we set **A** as NSD by setting $a = 0$, where the eigenvalues of **A** locate in $[-9.0266, 0]$. In (b), we generate BA network with **A** being ID by setting $a = 5$, where the eigenvalues of **A** locate in $[-5.0028, 5]$.

and

$$\begin{aligned} \underline{\beta} \approx \sum_{i=1}^{l}\sum_{j=1}^{l} \Bigg[\sum_{r=1}^{l} & \frac{16\lambda_r^2\lambda_i\lambda_j}{p_{hr}^2 p_{hi}p_{hj}(\lambda_r+\lambda_i)(\lambda_r+\lambda_j)} \\ & \cdot \prod_{k=1,k\neq r}^{n} \left(\frac{\lambda_r+\lambda_k}{\lambda_r-\lambda_k}\right)^2 \prod_{k=1,k\neq i}^{n} \frac{\lambda_i+\lambda_k}{\lambda_i-\lambda_k} \prod_{k=1,k\neq j}^{n} \frac{\lambda_j+\lambda_k}{\lambda_j-\lambda_k} \Bigg]^2. \end{aligned} \tag{A10}$$

In addition, both $\underline{\alpha}$ and $\underline{\beta}$ are constants independent of t_f and so $\overline{E}$ is.

Considering that trace$[(\mathbf{M}_1^{-1})^2]$ and trace$[(\mathbf{M}_1^{-1})^4]$ are employed to approximate $\underline{\alpha}$ and $\underline{\beta}$ in the cases of **A** being NSD and ID, we perform some numerical calculations to verify our analytical results (Fig. 6).

d. **A** *is PSD*

For large t_f, if **A** is PSD with $\lambda_1 = \cdots = \lambda_l = 0, 0 < \lambda_{l+1} \leqslant \cdots \leqslant \lambda_n$, then the component of $e^{4\lambda_n t_f}$ in (9) is dominant for $\overline{\alpha}$. Hence, $\overline{\alpha} \approx \frac{p_{hn}^4}{4\lambda_n^2} e^{4\lambda_n t_f}$ holds and, analogously, $\overline{\beta} \approx \frac{p_{hn}^8}{16\lambda_n^4} e^{8\lambda_n t_f}$ holds, as well as $\underline{E} \approx \frac{2\lambda_n}{p_{hn}^2} e^{-2\lambda_n t_f}$.

TABLE III. The lower bound of energy for one driver node.

		Large t_f				
Cases	Small t_f	**A** ND	**A** NSD	**A** ID	**A** PSD	**A** PD
$\overline{\alpha}$	$\sim t_f^2$	(A1)	$\sim t_f^2$	$\sim e^{4\lambda_n t_f}$	$\sim e^{4\lambda_n t_f}$	$\sim e^{4\lambda_n t_f}$
$\overline{\beta}$	$\sim t_f^4$	(A2)	$\sim t_f^4$	$\sim e^{8\lambda_n t_f}$	$\sim e^{8\lambda_n t_f}$	$\sim e^{8\lambda_n t_f}$
$\lambda_{\max}(\mathbf{M})$	$\sim t_f$	(5) with (A1) (A2)	$\sim t_f$	$\sim e^{2\lambda_n t_f}$	$\sim e^{2\lambda_n t_f}$	$\sim e^{2\lambda_n t_f}$
$\underline{E}$	$\sim t_f^{-1}$	(8) with (A1) (A2)	$\sim t_f^{-1}$	$\sim e^{-2\lambda_n t_f}$	$\sim e^{-2\lambda_n t_f}$	$\sim e^{-2\lambda_n t_f}$

TABLE IV. The upper bound of energy for one driver node.

Cases	Small t_f	Large t_f				
		A PD	**A** PSD	**A** ID	**A** NSD	**A** ND
$\underline{\alpha}$	$\sim t_f^{-2(N_0-N_{\min})}$	$\sim e^{-4\lambda_1 t_f}$	$\sim (t_f^{-1})^2$	(A9)	(A7)	(A3)
$\underline{\beta}$	$\sim t_f^{-4(N_0-N_{\min})}$	$\sim e^{-8\lambda_1 t_f}$	$\sim (t_f^{-1})^4$	(A10)	(A8)	(A4)
$\lambda_{\min}(\mathbf{M})$	$\sim t_f^{(N_0-N_{\min})}$	$\sim e^{2\lambda_1 t_f}$	$\sim t_f$	(6) with (A9) (A10)	(6) with (A7) (A8)	(6) with (A3) (A4)
$\overline{E}$	$\sim t_f^{-(N_0-N_{\min})}$	$\sim e^{-2\lambda_1 t_f}$	$\sim t_f^{-1}$	(7) with (A9) (A10)	(7) with (A7) (A8)	(7) with (A3) (A4)

Moreover, $\mathbf{M}$ can be given by

$$\mathbf{M} = \begin{bmatrix} \mathbf{M}_1 & \mathbf{M}_2 \\ \mathbf{M}_2^T & \mathbf{M}_3 \end{bmatrix}$$

with

$$\begin{cases} \mathbf{M}_1(i,j) = p_{hi}p_{hj}t_f, & i,j = 1,2,\ldots,l; \\ \mathbf{M}_2(i,j) = \frac{p_{hi}p_{hj}}{\lambda_j} e^{\lambda_j t_f}, & i = 1,2,\ldots,l;\ j = l+1,\ldots,n; \\ \mathbf{M}_3(i,j) = \frac{p_{hi}p_{hj}}{\lambda_i+\lambda_j} e^{(\lambda_i+\lambda_j)t_f}, & i,j = l+1,\ldots,n. \end{cases}$$

Similarly, for large t_f, we have $|\mathbf{M}| \sim e^{2(\lambda_{l+1}+\lambda_{l+2}+\cdots+\lambda_n)t_f} \cdot t_f^l$. In addition, it is clear that

$$\mathbf{M}_{ij} \sim \begin{cases} e^{2(\lambda_{l+1}+\lambda_{l+2}+\cdots+\lambda_n)t_f} \cdot t_f^{l-1}, & i,j \leqslant l; \\ e^{2(\lambda_{l+1}+\lambda_{l+2}+\cdots+\lambda_n)t_f-\lambda_j t_f} \cdot t_f^{l-1}, & i \leqslant l, j > l; \\ e^{2(\lambda_{l+1}+\lambda_{l+2}+\cdots+\lambda_n)t_f-\lambda_i t_f} \cdot t_f^{l-1}, & j \leqslant l, i > l; \\ e^{2(\lambda_{l+1}+\lambda_{l+2}+\cdots+\lambda_n)t_f-(\lambda_i+\lambda_j)t_f} \cdot t_f^{l}, & i,j > l. \end{cases}$$

Therefore, $\mathbf{M}^{-1}$ is

$$\mathbf{M}^{-1}(i,j) = \frac{\mathbf{M}_{ij}}{|\mathbf{M}|} \sim \begin{cases} t_f^{-1}, & i,j \leqslant l; \\ e^{-\lambda_j t_f} t_f^{-1}, & i \leqslant l, j > l; \\ e^{-\lambda_i t_f} t_f^{-1}, & j \leqslant l, i > l; \\ e^{-(\lambda_i+\lambda_j)t_f}, & i,j > l. \end{cases}$$

Since $\frac{e^{-\lambda_i t_f} t_f^{-1}}{t_f^{-1}} \to 0$ and $\frac{e^{-(\lambda_i+\lambda_j)t_f}}{t_f^{-1}} \to 0$ when $\lambda_i > 0$ and t_f is large, we have $\underline{\alpha} \sim (t_f^{-1})^2$, $\underline{\beta} \sim (t_f^{-1})^4$. Moreover, as shown in Table I, the upper bound of the energy is $\underline{E} \sim e^{-2\lambda_n t_f}$, and the upper bound of energy is $\overline{E} \sim t_f^{-1}$.

e. **A** *is PD*

For large t_f, if $\mathbf{A}$ is PD with $0 < \lambda_1 \leqslant \cdots \leqslant \lambda_n$, then we have $\underline{E} \sim e^{-2\lambda_n t_f}$. Matrix $\mathbf{M}$ of this case is given by $m_{ij} = \frac{p_{hi}p_{hj}}{\lambda_i+\lambda_j} e^{(\lambda_i+\lambda_j)t_f}$ for $i,j = 1,2,\ldots,n$. In the same way, we get $|\mathbf{M}| \sim e^{2(\lambda_1+\lambda_2+\cdots+\lambda_n)t_f}$ and $\mathbf{M}_{ij} \sim e^{2(\lambda_1+\lambda_2+\cdots+\lambda_n)t_f-(\lambda_i+\lambda_j)t_f}$. And then by $\frac{\mathbf{M}_{ij}}{|\mathbf{M}|} \sim e^{-(\lambda_i+\lambda_j)t_f}$ and $\frac{e^{-(\lambda_{i2}+\lambda_{j2})t_f}}{e^{-(\lambda_{i1}+\lambda_{j1})t_f}} \to 0$ for $\lambda_{i1}+\lambda_{j1} > \lambda_{i2}+\lambda_{j2}$, we have $\underline{\alpha} \sim e^{-4\lambda_1 t_f}$ and $\underline{\beta} \sim e^{-8\lambda_1 t_f}$. Hence, we have $\overline{E} \sim e^{-2\lambda_1 t_f}$.

Finally, we also summary the aforementioned results in Table III.

APPENDIX B: *d* DRIVER NODES

In this case, $\overline{\alpha}$ and $\overline{\beta}$ are given by

$$\begin{aligned} \overline{\alpha} &= \|\mathbf{M}\|_F^2 = \mathrm{trace}(\mathbf{M}^2) \\ &= \sum_{i=1}^{n}\sum_{j=1}^{n} \frac{\left(\sum_{k=1}^{d} p_{m_k i} p_{m_k j}\right)^2}{(\lambda_j+\lambda_i)^2} [e^{(\lambda_j+\lambda_i)t_f} - 1]^2 \end{aligned}$$

and

$$\begin{aligned} \overline{\beta} &= \mathrm{trace}(\mathbf{M}^4) \\ &= \sum_{i=1}^{n}\sum_{r=1}^{n} \left\{ \sum_{k=1}^{n} \frac{\left(\sum_{l=1}^{d} p_{m_l k} p_{m_l i}\right)\left(\sum_{l=1}^{d} p_{m_l k} p_{m_l r}\right)}{(\lambda_k+\lambda_i)(\lambda_k+\lambda_r)} \right. \\ &\quad \left. \cdot [e^{(\lambda_k+\lambda_i)t_f} - 1][e^{(\lambda_k+\lambda_r)t_f} - 1] \right\}^2. \end{aligned}$$

With an approximation $e^{(\lambda_i+\lambda_j)t_f} \approx 1 + (\lambda_i+\lambda_j)t_f$ for small t_f, we have

$$\overline{\alpha} = \|\mathbf{M}\|_F^2 \approx \sum_{i=1}^{n}\sum_{j=1}^{n} \left(\sum_{k=1}^{d} p_{m_k i} p_{m_k j} \right)^2 t_f^2 \tag{B1}$$

and

$$\begin{aligned} \overline{\beta} &= \|\mathbf{M}^2\|_F^2 \\ &\approx \sum_{i=1}^{n}\sum_{r=1}^{n} \left[\sum_{k=1}^{n} \left(\sum_{l=1}^{d} p_{m_l k} p_{m_l i} \right)\left(\sum_{l=1}^{d} p_{m_l k} p_{m_l r} \right) \right]^2 t_f^4. \end{aligned} \tag{B2}$$

TABLE V. The lower bound of energy for d driver nodes.

Cases	Small t_f	Large t_f		
		A ND	**A** NSD	**A** not ND
$\overline{\alpha}$	(B1)$\sim t_f^2$	(B3)	(B5)$\sim t_f^2$	(B7)$\sim e^{4\lambda_n t_f}$
$\overline{\beta}$	(B2)$\sim t_f^4$	(B4)	(B6)$\sim t_f^4$	(B8)$\sim e^{8\lambda_n t_f}$
$\lambda_{\max}(\mathbf{M})$	(5) with (B1) (B2)$\sim t_f$	(5) with (B3) (B4)	(5) with (B5) (B6) $\sim t_f$	(5) with (B7) (B8)$\sim e^{2\lambda_n t_f}$
$\underline{E}$	(8) with (B1) (B2)$\sim t_f^{-1}$	(8) with (B3) (B4)	(8) with (B5) (B6) $\sim t_f^{-1}$	(8) with (B7) (B8)$\sim e^{-2\lambda_n t_f}$

When **A** is ND for large t_f, we have

$$\overline{\alpha} = \|\mathbf{M}\|_F^2 \approx \sum_{i=1}^{n}\sum_{j=1}^{n} \frac{\left(\sum_{k=1}^{d} p_{m_k i} p_{m_k j}\right)^2}{(\lambda_j + \lambda_i)^2} \tag{B3}$$

and

$$\overline{\beta} = \mathrm{trace}(\mathbf{M}^4) \approx \sum_{i=1}^{n}\sum_{r=1}^{n}\left[\sum_{k=1}^{n} \frac{\left(\sum_{l=1}^{d} p_{m_l k} p_{m_l i}\right)\left(\sum_{l=1}^{d} p_{m_l k} p_{m_l r}\right)}{(\lambda_k + \lambda_i)(\lambda_k + \lambda_r)}\right]^2. \tag{B4}$$

When **A** is NSD for large t_f, we have

$$\overline{\alpha} = \|\mathbf{M}\|_F^2 \approx \sum_{i=1}^{n}\sum_{j=1}^{n}\left(\sum_{k=1}^{d} p_{m_k i} p_{m_k j}\right)^2 t_f^2 \tag{B5}$$

and

$$\overline{\beta} \approx \sum_{i=1}^{n}\sum_{r=1}^{n}\left[\sum_{k=1}^{n}\left(\sum_{l=1}^{d} p_{m_l k} p_{m_l i}\right)\left(\sum_{l=1}^{d} p_{m_l k} p_{m_l r}\right)\right]^2 t_f^4. \tag{B6}$$

TABLE VI. The upper bound of energy d driver nodes.

Cases	Small t_f	Large t_f		
		A PD	**A** PSD	**A** not PD
$\underline{\alpha}$	$\sim t_f^{-2(N_0'-N_{\min}')}$	$\sim e^{-4\lambda_1 t_f}$	$\sim (t_f^{-1})^2$	Constant
$\underline{\beta}$	$\sim t_f^{-4(N_0'-N_{\min}')}$	$\sim e^{-8\lambda_1 t_f}$	$\sim (t_f^{-1})^4$	Constant
$\lambda_{\min}(\mathbf{M})$	$\sim t_f^{(N_0'-N_{\min}')}$	$\sim e^{2\lambda_1 t_f}$	$\sim t_f$	Constant
$\overline{E}$	$\sim t_f^{-(N_0'-N_{\min}')}$	$\sim e^{-2\lambda_1 t_f}$	$\sim t_f^{-1}$	Constant

When **A** is not ND for large t_f, we have

$$\overline{\alpha} \approx \left(\frac{\sum_{k=1}^{d} p_{m_k n} p_{m_k n}}{2\lambda_n}\right)^2 e^{4\lambda_n t_f} \tag{B7}$$

and

$$\overline{\beta} \approx \left(\frac{\sum_{k=1}^{d} p_{m_k n} p_{m_k n}}{2\lambda_n}\right)^4 e^{8\lambda_n t_f}. \tag{B8}$$

The lower bound of energy for d driver nodes are presented in Table V. Analogously, we can get the upper bound of energy in different cases under d driver nodes as shown in Table VI.

[1] Y.-Y. Liu and A.-L. Barabási, Control principles of complex systems, Rev. Mod. Phys. **88**, 035006 (2016).

[2] A.-L. Barabási, *Network Science* (Cambridge University Press, Cambridge, 2016).

[3] B. Liu, T. Chu, L. Wang, and G. Xie, Controllability of a leader-follower dynamic network with switching topology, IEEE Trans. Autom. Control **53**, 1009 (2008).

[4] G. Xie and D. Zheng, Research on controllability and reachability of hybrid dynamical systems, Contl. Theor. Appl. **19**, 139 (2002).

[5] G. Xie and L. Wang, Controllability and stabilizability of switched linear-systems, Syst. Control Lett. **48**, 135 (2003).

[6] N. Masuda and R. Lambiotte, *A Guide to Temporal Networks* (World Scientific, Singapore, 2016).

[7] Y. Guan and L. Wang, Controllability of multi-agent systems with directed and weighted signed networks, Syst. Control Lett. **116**, 47 (2018).

[8] A. Li, S. P. Cornelius, Y.-Y. Liu, L. Wang, and A.-L. Barabási, The fundamental advantages of temporal networks, Science **358**, 1042 (2017).

[9] Y.-Y. Liu, J.-J. Slotine, and A.-L. Barabási, Controllability of complex networks, Nature **473**, 167 (2011).

[10] Z. Yuan, C. Zhao, Z. Di, W.-X. Wang, and Y.-C. Lai, Exact controllability of complex networks, Nat. Commun. **4**, 2447 (2013).

[11] T. Jia, Y.-Y. Liu, E. Csoka, M. Posfai, J.-J. Slotine, and A.-L. Barabási, Emergence of bimodality in controlling complex networks, Nat. Commun. **4**, 2002 (2013).

[12] A. Vinayagam, T. E. Gibson, H.-J. Lee, B. Yilmazel, C. Roesel, Y. Hu, Y. Kwon, A. Sharma, Y.-Y. Liu, N. Perrimon, and A.-L. Barabási, Controllability analysis of the directed human protein interaction network identifies disease genes and drug targets, Proc. Natl. Acad. Sci. USA **113**, 4976 (2016).

[13] J. Ruths and D. Ruths, Control profiles of complex networks, Science **343**, 1373 (2014).

[14] J. Gao, Y.-Y. Liu, R. M. D'Souza, and A.-L. Barabási, Target control of complex networks, Nat. Commun. **5**, 5415 (2014).

[15] T. Nepusz and T. Vicsek, Controlling edge dynamics in complex networks, Nat. Phys. **8**, 568 (2012).

[16] G. Yan, J. Ren, Y.-C. Lai, C.-H. Lai, and B. Li, Controlling Complex Networks: How Much Energy is Needed? Phys. Rev. Lett. **108**, 218703 (2012).

[17] F. Pasqualetti, S. Zampieri, and F. Bullo, Controllability metrics, limitations and algorithms for complex networks, IEEE Trans. Control Netw. Syst. **1**, 40 (2014).

[18] G. Yan, G. Tsekenis, B. Barzel, J.-J. Slotine, Y.-Y. Liu, and A.-L. Barabási, Spectrum of controlling and observing complex networks, Nat. Phys. **11**, 779 (2015).

[19] Y. Z. Chen, L. Z. Wang, W. X. Wang, and Y. C. Lai, Energy scaling and reduction in controlling complex networks, R. Soc. Open. Sci. **3**, 160064 (2016).

[20] A. Li, S. P. Cornelius, Y.-Y. Liu, L. Wang, and A.-L. Barabási, Control energy scaling in temporal networks, arXiv:1712.06434v1.

[21] A. Li, L. Wang, and F. Schweitzer, The optimal trajectory to control complex networks, arXiv:1806.04229.

[22] J. Sun and A. E. Motter, Controllability Transition and Nonlocality in Network Control, Phys. Rev. Lett. **110**, 208701 (2013).

[23] P. J. Antsaklis and A. N. Michel, *Linear Systems* (McGraw–Hill, New York, 1997).

[24] F. L. Lewis and V. L. Syrmos, *Optimal Control,* 2nd ed. (Wiley, New York, 1995).

[25] R. E. Kalman, Mathematical description of linear dynamical systems, J. Soc. Ind. Appl. Math. Ser. A **1**, 152 (1963).

[26] J. Lam, Z. Li, Y. Wei, J. Feng, and K. W. Chung, Estimates of the spectral condition number, Linear Multilinear A. **59**, 249 (2011).

[27] R. Albert, H. Jeong, and A. L. Barabási, Diameter of the world wide web, Nature **401**, 130 (1999).

[28] J.-M. Coron,*Control and Nonlinearity* (American Mathematical Society, 2009).

[29] P. Erdős and A. Rényi, On the evolution of random graphs, Publ. Math. Inst. Hungarian Acad. Sci. **5**, 17 (1960).